Performance analysis of quantum key distribution using polarized coherent-states in free-space channel

Zengte Zheng(郑增特)[1], Ziyang Chen(陈子扬)[2,†], Luyu Huang(黄露雨)[1], Xiangyu Wang(王翔宇)[1,‡], and Song Yu(喻松)[1]

[1] *State Key Laboratory of Information Photonics and Optical Communications, Beijing University of Posts and Telecommunications, Beijing* 100876, *China*

[2] *State Key Laboratory of Advanced Optical Communication Systems and Networks, School of Electronics, and Center for Quantum Information Technology, Peking University, Beijing* 100871, *China*

(Received 18 March 2022; revised manuscript received 9 May 2022; accepted manuscript online 29 May 2022)

In free space channel, continuous-variable quantum key distribution (CV-QKD) using polarized coherent-states can not only make the signal state more stable and less susceptible to interference based on the polarization non-sensitive of the free-space channel, but also reduce the noise introduced by phase interference. However, arbitrary continuous modulation can not be carried out in the past polarization coding, resulting in that the signal state can not obtain arbitrary continuous value in Poincare space, and the security analysis of CV-QKD using polarized coherent-states in free space is not complete. Here we propose a new modulation method to extend the modulation range of signal states with an optical-fiber-based polarization controller. In particular, in terms of the main influence factors in the free-space channel, we utilize the beam extinction and elliptical model when considering the transmittance and adopt the formulation of secret key rate. In addition, the performance of the proposed scheme under foggy weather is also taken into consideration to reveal the influence of severe weather. Numerical simulation shows that the proposed scheme is seriously affected by attenuation under foggy weather. The protocol fails when visibility is less than 1 km. At the same time, the wavelength can affect the performance of the proposed scheme. Specifically, under foggy weather, the longer the wavelength, the smaller the attenuation coefficient, and the better the transmission performance. Our proposed scheme can expand the modulation range of signal state, and supplement the security research of the scheme in the free-space channel, thus can provide theoretical support for subsequent experiments.

Keywords: polarized coherent-states, free-space channel, performance analysis

PACS: 03.67.Dd, 03.67.Hk, 03.67.–a **DOI:** 10.1088/1674-1056/ac7450

1. Introduction

Due to the non-cloning theorem,[1,2] quantum key distribution (QKD) technology has become a hot topic in the field of cryptography. Continuous-variable (CV) QKD[3–7] has attracted a lot of attention in the last few years, mainly because it is compatible with existing standard telecom components and can be used in common environments.[8–10] In recent decades, much experimental progress of CV-QKD has been made not only in optical-fiber links[11–18] but also in free-space channel.[19–31] However, usual CV-QKD with free-space channel suffers from the disadvantages that noise is easily introduced during spatial transmission and the signal state is particularly susceptible to turbulence.[32,33] Therefore, researchers use the polarization property of the beam for CV-QKD.[34] Compared with usual CV-QKD, CV-QKD using polarized coherent-states can not only make the signal state more stable and less susceptible to interference based on the polarization non-sensitive of free-space channel, but also reduce the noise introduced by phase interference.[23]

Compared to encoding in phase, CV-QKD using polarized coherent-states is not necessary to set local oscillator (LO) separately, but uses relatively bright $\hat{S}_1$ as LO.[23,34] In the past demonstration experiments, the polarized states of coherent beams were modulated by Alice using the electro-optic modulator (EOM),[23–29] then traveled through free space channel to Bob. Finally, Bob can directly measure the Stokes parameters of the beam using the combination of wave plates.[35,36] Nevertheless, in these experimental schemes, the Stokes parameter can not be modulated arbitrarily due to the limitation of modulation devices based on free space, so the signal states can not take arbitrary continuous values in Poincare sphere space. In addition, relevant security analysis[37–41] does not take into account the effects of foggy weather. Aiming at these problems, we propose a new modulation method to extend the modulation range of signal states with an optical-fiber-based polarization controller.[42] In particular, in terms of the main influence factors in the free-space channel, we utilize the beam extinction[43] and elliptical model[44] when considering the transmittance and adopt the formulation of secret key rate. At the same time, the effects of foggy weather on CV-QKD in free space are also taken into account, which has a greater impact than other severe weather.[45–48]

†Corresponding author. E-mail: chenziyang@pku.edu.cn
‡Corresponding author. E-mail: xywang@bupt.edu.cn

© 2023 Chinese Physical Society and IOP Publishing Ltd

In this paper, combined with the polarization controller based on optical fiber, the whole process of signal state change was studied and analyzed by using Muller matrix. It includes not only the modulation process of Alice, but also the heterodyne detection process of Bob. Then performance of CV-QKD using polarized coherent-states in free space is simulated and analyzed. Further, a comparison of the performance between the ideal case and practical case is revealed. Next, we utilize the channel model of foggy weather when considering influence of different degrees of foggy weather on our proposed scheme, and give the performance of CV-QKD with phase coding as a comparison. In addition, the influence of different wavelengths on our proposed scheme is also studied in the paper. These studies can extend the modulation range of signal states in the polarization coding experiment scheme and provide theoretical support for future experiments.

The rest of the paper is structured as follows. In Section 2, modulation method of the Stokes parameters and atmospheric CV-QKD model is introduced. Next in Section 3, the performance of CV-QKD using polarized coherent-states in free-space channel is simulated by combining the beam extinction and elliptical model. Then in Section 4, the performance of CV-QKD using polarized coherent-states under foggy weather is simulated and analyzed based on the characteristics of fog and the Mie scattering theory. Finally, we concludes the study of this paper in Section 5.

2. Atmospheric CV-QKD model and polarization encoding principle

2.1. Protocol description

The scheme of the protocol is given in Fig. 1. Firstly, Alice modulates the polarized state of the laser randomly. Since the atmospheric channel is polarization non-sensitive, the polarized state of the laser almost does not change when it reaches Bob through the atmospheric channel. And Bob characterizes the incoming light by a heterodyne measurement consisting of two polarization sensitive homodyne setups. Bob will perform projection measurement on the received signal. When the measurement is greater than 0, the mapping is 0, otherwise the mapping is 1. In the following process, the data measured by Bob is corrected to eliminate the influence of error code.

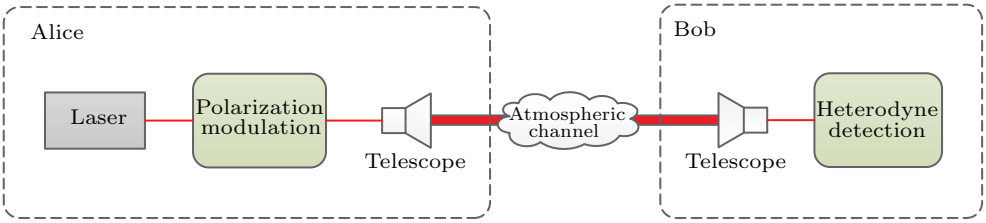


Fig. 1. Schematic diagram of prepare-and-measure CV-QKD using polarized coherent-states.

Unlike usual coherent-state CV-QKD protocol, our protocol makes use of the polarization properties of coherent states. The quantum Stokes operators are used throughout this work to describe the quantum polarization. They are defined in analogy to the classical Stokes parameters and the quantum Stokes operator is expressed as follows:[23,28,34,49]

$$\begin{aligned}\hat{S}_0 &= \hat{a}_{\mathrm{H}}^{\dagger}\hat{a}_{\mathrm{H}} + \hat{a}_{\mathrm{V}}^{\dagger}\hat{a}_{\mathrm{V}},\\ \hat{S}_1 &= \hat{a}_{\mathrm{H}}^{\dagger}\hat{a}_{\mathrm{H}} - \hat{a}_{\mathrm{V}}^{\dagger}\hat{a}_{\mathrm{V}},\\ \hat{S}_2 &= \hat{a}_{\mathrm{H}}^{\dagger}\hat{a}_{\mathrm{V}} + \hat{a}_{\mathrm{V}}^{\dagger}\hat{a}_{\mathrm{H}},\\ \hat{S}_3 &= \mathrm{i}\left(\hat{a}_{\mathrm{V}}^{\dagger}\hat{a}_{\mathrm{H}} - \hat{a}_{\mathrm{H}}^{\dagger}\hat{a}_{\mathrm{V}}\right),\end{aligned} \tag{1}$$

where H and V represent the horizontal and vertical directions, respectively. The Stokes uncertainty can be expressed as follows:

$$\left(\Delta\hat{S}_j\right)^2 \cdot \left(\Delta\hat{S}_k\right)^2 \geq \left|\langle\hat{S}_l\rangle\right|^2, \quad j \neq k \neq l. \tag{2}$$

Equation (2) indicates that as long as one Stokes operator is not zero, the other two Stokes operators cannot be measured simultaneously, similar to the uncertainty relationship of the momentum operator as well as the coordinate operator. However, the difference is that the uncertainty region of two Stokes operators is related to the third Stokes operator, while the uncertainty region of the momentum and coordinate operators is fixed.

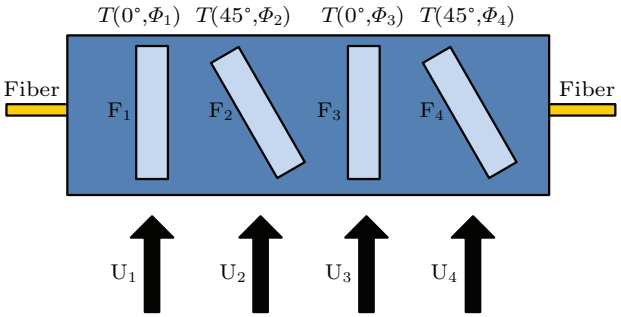


Fig. 2. Structure of polarization controller (for example PolaRIT E^{TM} II, General Photonics Co).

Therefore, we use polarization degree to encode information. Firstly, Alice generates a coherent beam which is strongly polarized in the x direction and the intensity is S_0. we can know that $\langle\hat{S}_1\rangle \approx \langle\hat{S}_0\rangle$, and $\langle\hat{S}_1\rangle \geq \langle\hat{S}_2\rangle, \langle\hat{S}_3\rangle$. So $\hat{S}_1$

polarized coherent-state light plays the role of local oscillator (LO), $\hat{S}_2$ and $\hat{S}_3$ polarized state generated by a modulation are two orthogonal quadratures. However, it is difficult to modulate the Stokes parameter of the beam arbitrarily with conventional modulation devices based on free space such as EOM. In this paper, the modulation method of Stokes parameter in CV-QKD using polarized coherent-states is studied by using polarization controller based on optical fiber.

The wave plates in the polarization controller have a fixed azimuthal angle and adjustable phase difference, where the first three wave plates are mainly combined to modulate the Stokes parameter of the beam arbitrarily and the fourth wave plate is set for reset-free problem. Assuming that the phase differences generated by the three wave plates are $2\phi_1, 2\phi_2, 2\phi_3$, and that the phase differences are all linear with respect to the applied voltage, which can turn out that the Jones matrices of the three wave plates can be expressed as follows:[42]

$$\boldsymbol{J}_{\phi_1} = \begin{pmatrix} \exp(\mathrm{j}\phi_1) & 0 \\ 0 & \exp(-\mathrm{j}\phi_1) \end{pmatrix}, \tag{3}$$

$$\boldsymbol{J}_{\phi_2} = \begin{pmatrix} \cos\phi_2 & -\mathrm{j}\sin\phi_2 \\ -\mathrm{j}\sin\phi_2 & \cos\phi_2 \end{pmatrix}, \tag{4}$$

$$\boldsymbol{J}_{\phi_3} = \begin{pmatrix} \exp(\mathrm{j}\phi_3) & 0 \\ 0 & \exp(-\mathrm{j}\phi_3) \end{pmatrix}, \tag{5}$$

the total transmission matrix when using three waveplates is expressed as follows:

$$\boldsymbol{J}_{\mathrm{tot}} = \begin{pmatrix} \cos\phi_2 \exp[\mathrm{j}(\phi_1+\phi_3)] & -\mathrm{j}\sin\phi_2 \exp[\mathrm{j}(\phi_3-\phi_1)] \\ -\mathrm{j}\sin\phi_2 \exp[\mathrm{j}(\phi_1-\phi_3)] & \cos\phi_2 \exp[-\mathrm{j}(\phi_1+\phi_3)] \end{pmatrix}, \tag{6}$$

its corresponding Muller matrix is computationally expressed as follows:

$$\boldsymbol{M}_{\mathrm{tot}} = \begin{pmatrix} \cos\phi_2 & \sin\phi_3\sin\phi_2 & -\cos\phi_1\sin\phi_2 \\ \sin\phi_2\sin\phi_3 & \cos\phi_1\cos\phi_3 - \sin\phi_1\sin\phi_3\cos\phi_2 & \sin\phi_1\cos\phi_3 + \sin\phi_3\cos\phi_2\cos\phi_1 \\ \sin\phi_2\cos\phi_3 & -\sin\phi_3\cos\phi_3 - \cos\phi_2\sin\phi_3\cos\phi_3 & \sin\phi_1\sin\phi_3 - \cos\phi_1\cos\phi_2\cos\phi_3 \end{pmatrix}. \tag{7}$$

After polarization controller, without loss of generality, the output light can be expressed by Muller matrix as follows:

$$\boldsymbol{M}_{\mathrm{Alice}} = S_0 \begin{pmatrix} 1 \\ \cos\phi_2 \\ -\sin\phi_2\sin\phi_3 \\ -\sin\phi_2\cos\phi_3 \end{pmatrix}. \tag{8}$$

The beam reaches Bob after passing through the free-space channel, and Bob performs heterodyne detection and realizes the demodulation of the beam through the combination of half wave plate, quarter wave plate and polarization beam splitter (PBS) wave plate. Assuming that the polarized state of the input at Bob is expressed as

$$\boldsymbol{M}_{\mathrm{Input}} = \begin{pmatrix} S_0 \\ S_1 \\ S_2 \\ S_3 \end{pmatrix}. \tag{9}$$

The Muller matrix representation of the half-wave and quarter-wave slices is obtained by calculation as follows:

$$\boldsymbol{M}_{\mathrm{H}} = \begin{pmatrix} 1 & 0 & 0 & 0 \\ 0 & \cos 4\theta & \sin 4\theta & 0 \\ 0 & \sin 4\theta & -\cos 4\theta & 0 \\ 0 & 0 & 0 & -1 \end{pmatrix}, \tag{10}$$

$$\boldsymbol{M}_{\mathrm{Q}} = \begin{pmatrix} 1 & 0 & 0 & 0 \\ 0 & \cos^2 2\theta & \cos 2\theta\sin\theta & -\sin 2\theta \\ 0 & \cos 2\theta\sin\theta & \sin^2 2\theta & \cos 2\theta \\ 0 & \sin 2\theta & -\cos 2\theta & 0 \end{pmatrix}. \tag{11}$$

After PBS, the following matrices are used for calculation:

$$\boldsymbol{M}_{\mathrm{PBS_H}} = \frac{1}{2}\begin{pmatrix} 1 & 1 & 0 & 0 \\ 1 & 1 & 0 & 0 \\ 0 & 0 & 0 & 0 \\ 0 & 0 & 0 & 0 \end{pmatrix}, \tag{12}$$

$$\boldsymbol{M}_{\mathrm{PBS_V}} = \frac{1}{2}\begin{pmatrix} 1 & -1 & 0 & 0 \\ -1 & 1 & 0 & 0 \\ 0 & 0 & 0 & 0 \\ 0 & 0 & 0 & 0 \end{pmatrix}, \tag{13}$$

where H and V represent the horizontal and vertical directions, respectively.

To obtain polarized state $\hat{S}_2$, Bob performs heterodyne detection and demodulation to obtain the Muller matrix as follows:

$$\begin{aligned} &\boldsymbol{M}_{\mathrm{PBS_H}} \cdot \boldsymbol{M}_{\mathrm{H}} \cdot \boldsymbol{M}_{\mathrm{Input}} - \boldsymbol{M}_{\mathrm{PBS_V}} \cdot \boldsymbol{M}_{\mathrm{H}} \cdot \boldsymbol{M}_{\mathrm{Input}} \\ &= \begin{pmatrix} \cos 4\theta \cdot S_1 + \sin 4\theta \cdot S_2 \\ S_0 \\ 0 \\ 0 \end{pmatrix}. \end{aligned} \tag{14}$$

With $\theta = 22.5^\circ$, the matrix corresponding to the half wave plate is expressed as

$$\boldsymbol{M}_{\mathrm{H}} = \begin{pmatrix} 1 & 0 & 0 & 0 \\ 0 & 0 & 1 & 0 \\ 0 & 1 & 0 & 0 \\ 0 & 0 & 0 & -1 \end{pmatrix}. \tag{15}$$

Thus Bob can obtain polarized state $\hat{S}_2$ by the following

Muller matrix:

$$\boldsymbol{M}_{\mathrm{PBS_H}}\cdot\boldsymbol{M}_{\mathrm{H}}\cdot\boldsymbol{M}_{\mathrm{Input}}-\boldsymbol{M}_{\mathrm{PBS_V}}\cdot\boldsymbol{M}_{\mathrm{H}}\cdot\boldsymbol{M}_{\mathrm{Input}}=\begin{pmatrix}S_2\\S_0\\0\\0\end{pmatrix}. \quad (16)$$

Substituting the modulated data at Alice, the polarized state $\hat{S}_2$ after detection can be obtained as $-S_0\sin\phi_2\sin\phi_3$. Similarly, the polarized state $\hat{S}_3$ measured by Bob is $-S_0\sin\phi_2\cos\phi_3$.

In order to obtain Stokes parameters $\hat{S}_2$ and $\hat{S}_3$ satisfying the Gaussian distribution in the experiment, the phase difference of the wave plate in the polarization controller should be modulated firstly, and the probability density of $\hat{S}_2$ and $\hat{S}_3$ is expressed as follows:

$$p\left(\hat{S}_2\right)=\frac{1}{\sqrt{2\pi\sigma^2}}\exp\left(-\frac{\hat{S}_2^2}{2\sigma^2}\right), \quad (17)$$

$$p\left(\hat{S}_3\right)=\frac{1}{\sqrt{2\pi\sigma^2}}\exp\left(-\frac{\hat{S}_3^2}{2\sigma^2}\right). \quad (18)$$

Since $\hat{S}_2$ and $\hat{S}_3$ are independent, the joint probability density function is

$$\begin{aligned}p_{\hat{S}_2,\hat{S}_3}\left(\hat{S}_2,\hat{S}_3\right)&=p\left(\hat{S}_2\right)p\left(\hat{S}_3\right)\\&=\frac{1}{\sqrt{2\pi\sigma^2}}\exp\left(-\frac{\hat{S}_2^2+\hat{S}_3^2}{2\sigma^2}\right).\end{aligned} \quad (19)$$

With $\hat{S}_2=-\sin\phi_2\sin\phi_3$, $\hat{S}_3=-\sin\phi_2\cos\phi_3$, we have

$$p\left(\phi_2,\phi_3\right)=p_{\hat{S}_2,\hat{S}_3}\left(\hat{S}_2,\hat{S}_3\right)|J|, \quad (20)$$

where

$$\begin{aligned}|\boldsymbol{J}|&=\begin{vmatrix}\frac{\partial\hat{S}_2}{\partial\phi_2}&\frac{\partial\hat{S}_3}{\partial\phi_2}\\\frac{\partial\hat{S}_2}{\partial\phi_3}&\frac{\partial\hat{S}_3}{\partial\phi_3}\end{vmatrix}=\begin{vmatrix}-\cos\phi_2\sin\phi_3&-\cos\phi_2\sin\phi_3\\-\sin\phi_2\cos\phi_3&\sin\phi_2\sin\phi_3\end{vmatrix}\\&=-\frac{1}{2}\sin2\phi_2.\end{aligned} \quad (21)$$

The joint probability distribution of ϕ_2 and ϕ_3 can be expressed as follows, and ϕ_2 and ϕ_3 are independent

$$p\left(\phi_2,\phi_3\right)=\frac{\sin2\phi_2}{4\pi\sigma^2}\exp\left(\frac{\cos2\phi_2}{4\sigma^2}\right)\exp(-1). \quad (22)$$

Assuming that ϕ_2 and ϕ_3 satisfy the following probability distribution, $\hat{S}_2$ and $\hat{S}_3$ satisfy the Gaussian distribution, respectively

$$p\left(\phi_2\right)=\frac{\sin2\phi_2}{2\sigma^2}\exp\left(\frac{\cos2\phi_2}{4\sigma^2}\right), \quad (23)$$

$$p\left(\phi_3\right)=\frac{1}{2\pi\sigma^2}\exp(-1). \quad (24)$$

2.2. Free-space channel model

The effect of the atmospheric channel on QKD can be divided into two main cases (for details see Appendix A): beam extinction and turbulence. Atmospheric turbulence causes random changes in the transmittance of laser transmission in atmospheric channels mainly through its influence on beam drift, broadening and deformation. The elliptic model can greatly simplify the analysis of the above effects of turbulence.

In the elliptic model, a set of parameter vector $\boldsymbol{v}=(x_0,y_0,W_1,W_2,\varphi_0)$ is used to describe the beam state on the receiving plane. Wherein, (x_0,y_0) represents the position of light spot on the transmission cross section, W_1 and W_2 represent the long and short axes of elliptical beam respectively, and φ_0 represents the relative angle between the new coordinate system and the original coordinate system. The coordinate parameter (x_0,y_0) can be transformed into polar coordinate $(r_0\cos\varphi_0,r_0\sin\varphi_0)$, and r_0 represents the relative position of the new coordinate system and the original coordinate system based on the location of the light spot.

Define $\zeta=\phi-\varphi_0$, then the formula for transmittance can be expressed as

$$T_{\mathrm{ell}}=T_{\mathrm{ell},0}\exp\left\{-\left[\frac{r_0/a}{R\left(\frac{2}{W_{\mathrm{eff}}(\zeta)}\right)}\right]^{Q\left(\frac{2}{W_{\mathrm{eff}}(\zeta)}\right)}\right\}, \quad (25)$$

where ϕ represents the angle between the long axis and the x' axis of the elliptical beam in the new coordinate system, $\phi\in[0,\pi/2)$, and specific expressions of the other parameters are shown in Appendix B.

According to the elliptical model, the probability distribution of transmittance can be calculated by generating a large number of random numbers using the Monte–Carlo method. Where ϕ satisfies a uniform distribution, the coordinates x_0 and y_0 both satisfy a normal distribution with mean value 0, and the long and short axes satisfy a normal distribution.

Because of the high directivity of laser transmission, when the arrival angle fluctuates greatly, the communication is interrupted when the focus is not in the core of the receiving fiber.

Since the offset angle is extremely small, $\sin\beta_{\mathrm{a}}\cong\beta_{\mathrm{a}}$, and because of the close relationship between beam drift and interference, β_{a} satisfies a normal distribution with mean value of 0

$$\left\langle\beta_{\mathrm{a}}^2\right\rangle=\frac{\left\langle\Delta x_0^2\right\rangle}{L^2}. \quad (26)$$

Therefore, the interruption probability can be calculated by the following equation:

$$P=1-\int_{-d_{\mathrm{cor}}/2}^{d_{\mathrm{cor}}/2}\frac{1}{\sqrt{2\pi\left\langle\beta_{\mathrm{a}}^2\right\rangle}f}\exp\left(\frac{-l^2}{2f^2\left\langle\beta_{\mathrm{a}}^2\right\rangle}\right)\mathrm{d}l, \quad (27)$$

where d_{cor} denotes the fiber diameter in meters.

Combined with the probability of interruption P that exists in free space, the secret key rate G under collective attack with reverse reconciliation efficiency β is given as

$$G = (1-P)(\beta I_{\mathrm{AB}} - \chi_{\mathrm{BE}}). \tag{28}$$

Assuming no noise in the channel, the secret key rate using polarized coherent-states can be calculated using the following equation:[50]

$$G = (1-P)\int_0^{\infty} 2\mathrm{d}\beta_x p(\beta_x) \times \left[\beta\left(1-H^{\mathrm{bin}}(\mathrm{err})\right) - \chi(\beta_x)\right], \tag{29}$$

where β_x represents the value in $|\beta\rangle = |\beta_x + \mathrm{i}\beta_y\rangle$ obtained by Bob through projection measurement, $p(\beta_x)$ represents the probability that Bob gets β_x by heterodyne detection, $H^{\mathrm{bin}}(\mathrm{err})$ represents the entropy of a binary symmetric channel derived from the error rate, and $\chi(\beta_x)$ represents the Holevo quantity under reverse reconciliation.

In this paper, the performance of CV-QKD using polarized coherent-states in free channel is simulated with beam extinction and elliptical model. The simulation parameters of receiving lens radius, transmitting lens radius, laser wavelength, fiber core diameter, modulation variance, and atmospheric turbulence at outer and inner scales are set as shown in Table 1. Based on the ideal situation, we set the reverse reconciliation efficiency as 100%, and assume that there is no noise in the detection. Other atmospheric parameters are shown in Tables A1 and A2.

Table 1. The parameters setting for performance analysis.

Parameters	Values	Description
a	110 mm	receiving lens radius
W_0	80 mm	transmitting lens radius
λ	1550 nm	laser wavelength
d_{cor}	9 μm	fiber core diameter
l_0	4 mm	inner scale of atmosphere
L_0	0.4 m	outer scale of atmosphere
V_{A}	0.8 SNU	modulation variance

3. Security analysis of CV-QKD in free space channel

Figure 3 shows the relationship between transmittance and distance in different seasons, from which it can be seen that the effect of turbulence is not very obvious within 4 km, but becomes more obvious as the distance increases. In the longer distance transmission, since the turbulence intensity is stronger in winter than in summer, the transmittance decreases faster with increasing distance in winter.

The effect of the interruption probability on the secret key rate during longer distance transmission in different seasons is simulated in Fig. 4. The circles represent the ideal case and the triangle represents the secret key rate, where the signal in the channel may be interrupted to some extent. It can be observed that the interruption probability of the beam in the channel does not affect the secret key rate during longer distance transmission in summer. The transmission distance is longer and the secret key rate is higher due to the weaker turbulence intensity in summer. In contrast, during winter, the interruption probability does not affect the secret key rate at short transmission distance, and at longer transmission distance, the interruption probability makes the secret key rate start to decrease, and when the transmission distance reaches its maximum, the effect of the interruption probability starts to decrease again. This is mainly due to the fact that the effect of turbulence is not particularly pronounced at short transmission distance, and the effect of interruption probability on CV-QKD using polarized coherent-states starts to decrease again at the longest transmission distance.

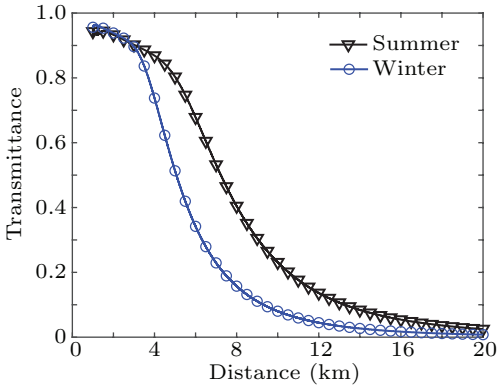


Fig. 3. The relationship between transmittance and distance in different seasons.

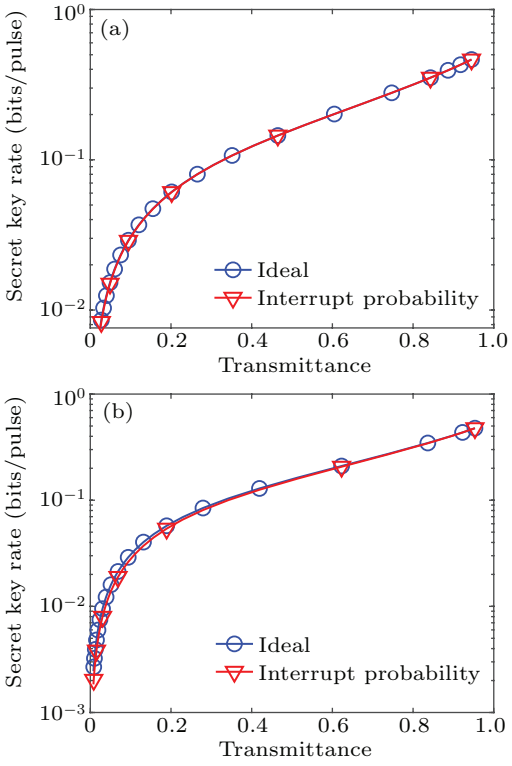


Fig. 4. Influence of interruption probability on the secret key rate of CV-QKD using polarized coherent-states in different seasons: (a) summer and (b) winter.

In practical experiments, detector noise is an important factor which can not be ignored. Therefore, the influence of different detector noise on the secret key rate is considered in Fig. 5. The triangle represents the ideal situation where the detector without noise, and the star and circle represent the secret key rate when the detector noise is $\delta_{\text{det}} = 0.05$ and $\delta_{\text{det}} = 0.1$, respectively. As can be seen from the figure, with the increase of detector noise, the secret key rate begins to decline, but it does not affect the furthest transmission distance of CV-QKD using polarized coherent-states, and with the increase of transmission distance, the influence of detector noise on the secret key rate begins to weaken.

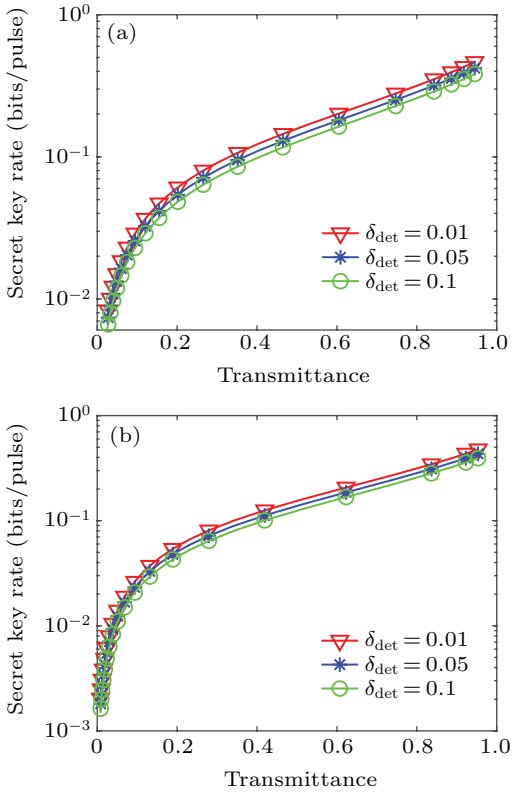


Fig. 5. Influence of detector noise on the secret key rate of CV-QKD using polarized coherent-states in different seasons: (a) summer and (b) winter.

4. Performance of CV-QKD under foggy weather

Laser transmission in free space always encounters various kinds of severe weather, such as rain, snow, fog, etc. However, since the scattering caused by rain and snow is non-selective scattering, and the scattering caused by foggy weather is Mie scattering, the foggy weather cause more severe attenuation to free space communication compared to other severe weather. Therefore, the performance of CV-QKD using polarized coherent-states under foggy weather is simulated and analyzed in this paper.

The attenuation of laser transmission under foggy weather can be described by the fog channel attenuation correction formula proposed by Kim *et al.* in 2001[51]

$$\alpha_{\text{fog}} = \frac{3.91}{V_{\text{fog}}}\left(\frac{\lambda}{550}\right)^{-q}, \tag{30}$$

where q varies with different values of visibility V_{fog},

$$q = \begin{cases} 1.6, & V_{\text{fog}} > 50 \text{ km}, \\ 1.3, & 6 \text{ km} < V_{\text{fog}} < 50 \text{ km}, \\ 0.16V_{\text{fog}} + 0.34, & 1 \text{ km} < V_{\text{fog}} < 6 \text{ km}, \\ V_{\text{fog}} - 0.5, & 0.5 \text{ km} < V_{\text{fog}} < 1 \text{ km}, \\ 0, & V_{\text{fog}} < 0.5 \text{ km}. \end{cases} \tag{31}$$

We set visibility V_{fog} equal to 5 km refers to light fog, and V_{fog} equal to 1 km refers to heavy fog. Figure 6 simulates the relationship between transmittance and distance in the channel on foggy days of different seasons and degrees. The triangle represents the change of transmittance in the real channel under good weather conditions, the asterisk represents the light fog situation when V_{fog} is equal to 5 km, and the circle represents the heavy fog situation when V_{fog} is equal to 1 km. As can be seen in Fig. 6, compared to the free-space channel in good weather, there has been a greater attenuation in the light fog case at V_{fog} is equal to 5 km. When the visibility V_{fog} is equal to 1 km, the channel transmittance has become small at 2 km, with the effect of turbulence is small at this time, and the transmittance is mainly affected by attenuation caused by the foggy weather.

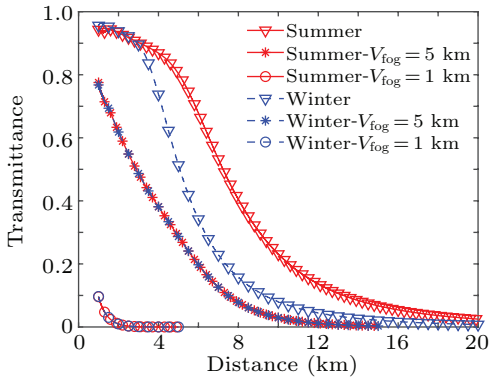


Fig. 6. The relationship between transmittance and distance in different season and degree of fog.

Figure 7 shows the secret key rate under different levels of fog. Compared with Fig. 4, there is still a considerable secret key rate and transmission distance under light fog, but as the visibility drops to 1 km, it can be found from Fig. 8 that the fog fading rises exponentially at this time, and the secret key rate at 2 km is already very low. Meanwhile, we use the red curve in Fig. 7 to represent the performance of CV-QKD with phase coding in foggy weather when visibility is 5 km. As can be seen from the figure, turbulence intensity has a more obvious impact on phase coding than polarization coding, and polarization coding has a longer transmission distance and a relatively higher secret key rate than CV-QKD with phase coding in foggy conditions.

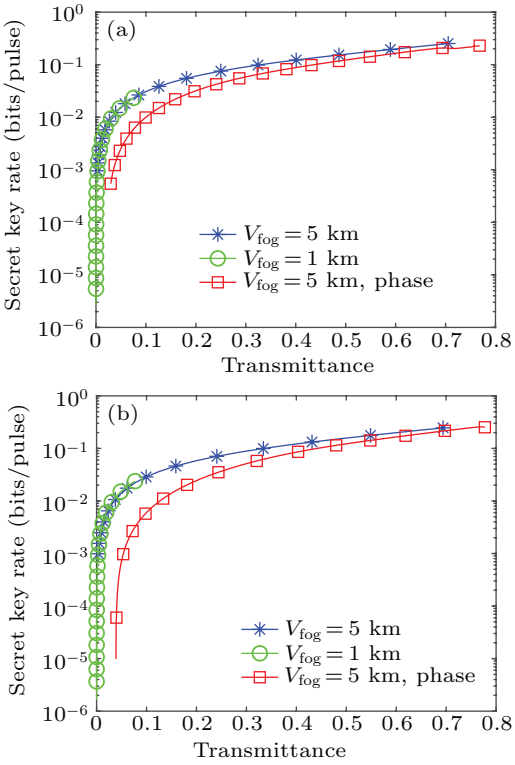


Fig. 7. The influence of different levels of visibility on secret key rate in different seasons: (a) summer and (b) winter.

Different wavelengths of laser will have different performance in the case of good visibility,[51,52] and Fig. 8 depicts the relationship between the attenuation coefficient and visibility foggy weather at different wavelengths. In the figure, the attenuation coefficient increases exponentially with visibility V_{fog} is smaller than 1 km, while visibility V_{fog} is greater than 1 km, the attenuation coefficient changes more smoothly. Compared with the 800 nm band, the attenuation of the laser in the 1550 nm band is lower during transmission. However, when V_{fog} is smaller than 500 m, the 1550 nm band laser does not have much advantage over the 800 nm band laser.

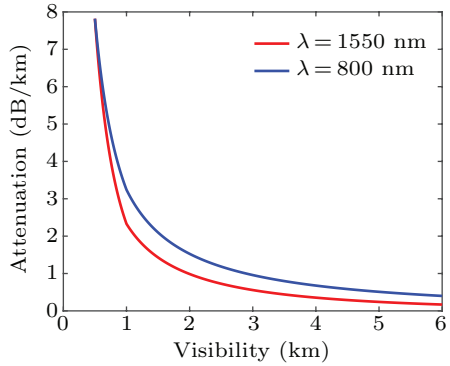


Fig. 8. Relationship between attenuation and visibility at different wavelengths.

Figure 9 simulates the channel transmittance at different wavelengths in different seasons under heavy fog at visibility V_{fog} is equal 1 km. As can be seen from the figure, when laser is transmitted over a short distance under foggy weather, the influence of turbulence is not great, and the influence of channel on QKD is mainly the strong attenuation brought by foggy weather. The red and blue colors in the figure represent summer and winter respectively, with the triangle and square represent the wavelengths of 1550 nm and 800 nm, respectively. Since the turbulence is not very influential in short-range transmission, the influence of different seasons on the channel transmittance is not very large, and the fading caused by foggy weather is the main factor for the secret key rate at this time.

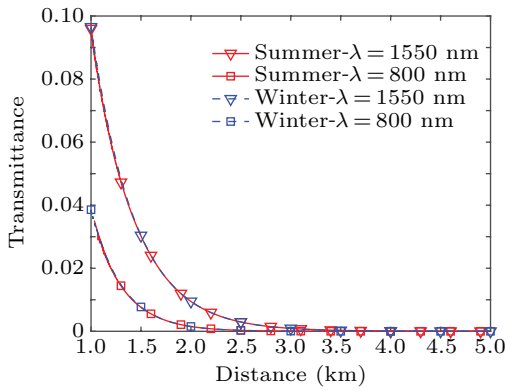


Fig. 9. The relationship between channel transmittance and distance at different wavelengths in different seasons when $V_{fog} = 1$ km.

The secret key rate of CV-QKD using polarized coherent-states is simulated based on the channel transmittance in Fig. 9, as shown in Fig. 10. Under the foggy weather with visibility of 1 km, 1550 nm shows better performance, with relatively higher obtained key rate and longer transmission distance.

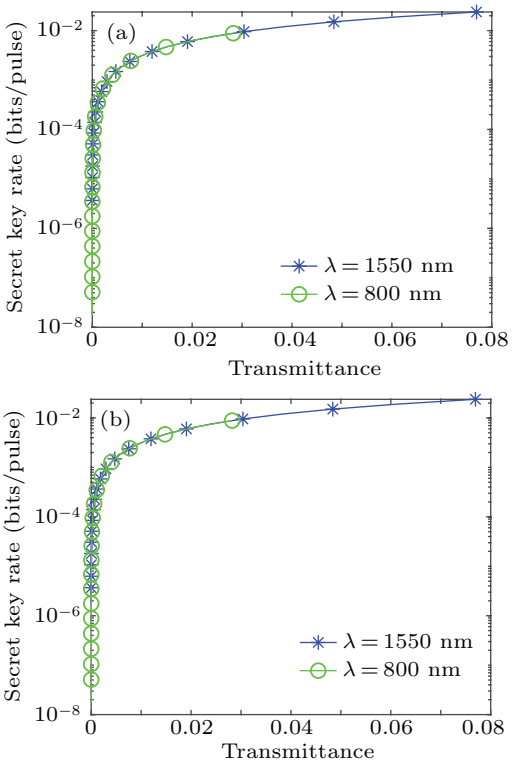


Fig. 10. The influence of different wavelengths on secret key rate in different seasons at $V_{fog} = 1$ km: (a) summer, (b) winter.

5. Conclusion

In this paper, a new modulation scheme is proposed, which enables the researchers to arbitrarily modulate the Stokes component of the beam in experiments, so as to allows the signal states to arbitrarily take continuous values in Poincare sphere space and enlarging the modulation range of the signal states. In particular, in terms of the main influence factors in the free-space channel, we utilize the beam extinction and elliptical model when considering the transmittance and adopt the formulation of secret key rate. Our results show that the turbulence intensity has a great influence on the secret key rate under good weather, both secret key rate and transmission distance decrease with the increase of turbulence intensity. However, turbulence and imperfect device factors does not affect the furthest transmission distance and the secret key rate under the farthest transmission distance. Besides, it will be affected by extremely serious attenuation when we perform the proposed scheme under foggy weather. If visibility is smaller than 1 km, the attenuation in free-space channel increases exponentially, and it is difficult to carry out CV-QKD. Meanwhile the farthest transmission distance of the proposed scheme is only about 2 km while visibility is equal to 1 km. Whereas visibility is greater than 1 km, the attenuation of different degrees of foggy weather has little change. At this time, the transmission distance and secret key rate of the proposed scheme are still considerable. Moreover, compared with phase coding CV-QKD, our proposed scheme has better performance under the same conditions in foggy weather. In addition, when the visibility is not less than 1 km, the longer the wavelength, the smaller the attenuation coefficient, the better the transmission performance. Our work expands the modulation range of signal states in the experimental scheme and analyzes the security of related protocols, which can provide theoretical support for future practical experiments.

Appendix A: Influence of free-space channel

The Rytov variance is employed to describe the strength of turbulence, and the equation is shown below:

$$\sigma_1^2 = 1.23 C_n^2 k^{7/6} L^{11/6}. \tag{A1}$$

As can be seen from the Table A1, the refractive index structure parameters in spring and summer are relatively similar, but the corresponding value in summer is a little larger. Meanwhile, winter and autumn are the two seasons with larger refractive index structure parameters, and winter is greater. Therefore, when considering the impact of turbulence intensity on quantum key distribution, summer can be taken as an example for weak turbulence, while winter weather conditions can be taken into account for strong turbulence.

The transmittance of the horizontal path can be expressed by[43]

$$T_{\text{ext}}(L) = \mathrm{e}^{-\alpha(\lambda)L}, \tag{A2}$$

where the total extinction coefficient includes aerosol scattering, aerosol absorption, molecular scattering and molecular absorption

$$\alpha(\lambda) = \alpha_{\text{sca}}^{\text{aer}}(\lambda) + \alpha_{\text{abs}}^{\text{aer}}(\lambda) + \alpha_{\text{sca}}^{\text{mol}}(\lambda) + \alpha_{\text{abs}}^{\text{mol}}(\lambda). \tag{A3}$$

Refractive index structure parameters C_n^2 and extinction coefficient α used in the simulation are from long-term measurements in Hefei, Anhui Province, China, as shown in Tables A1 and A2. The corresponding extinction coefficients in summer and winter are shown in Table A2.

Table A1. The C_n^2 values within the four-level boundary layer.

	Spring	Summer	Autumn	Winter
C_n^2 (10^{-15} m$^{-2/3}$)	2.03	2.12	5.56	7.46

Table A2. Extinction coefficients in km^{-1} for summer and winter.

Season	$\alpha_{\text{sca}}^{\text{aer}}(\lambda)$	$\alpha_{\text{abs}}^{\text{aer}}(\lambda)$	$\alpha_{\text{sca}}^{\text{mol}}(\lambda)$	$\alpha_{\text{abs}}^{\text{mol}}(\lambda)$
Summer	2.52×10^{-2}	5.49×10^{-3}	1.64×10^{-4}	3.35×10^{-3}
Winter	2.52×10^{-2}	5.49×10^{-3}	1.77×10^{-4}	8.56×10^{-3}

Appendix B: The parameters of T_{ell}

The $T_{\text{ell},0}$ represents the transmittance of the central beam, and the formula is expressed as follows:

$$\begin{aligned} T_{\text{ell},0} = {} & 1 - I_0\left(a^2\left[\frac{1}{W_1^2} - \frac{1}{W_2^2}\right]\right) \mathrm{e}^{-a^2\left(\frac{1}{W_1^2}+\frac{1}{W_2^2}\right)} \\ & - 2\left\{1 - \exp\left[-\frac{a^2}{2}\left(\frac{1}{W_1} - \frac{1}{W_2}\right)^2\right]\right\} \\ & \times \exp\left\{-\left[\frac{\frac{(W_1+W_2)^2}{\left|W_1^2 - W_2^2\right|}}{R\left(\frac{1}{W_1} - \frac{1}{W_2}\right)}\right]^{Q\left(\frac{1}{W_1} - \frac{1}{W_2}\right)}\right\}. \end{aligned} \tag{B1}$$

The $W_{\text{eff}}(\zeta)$ denotes the effective square radius of the light spot, and the formula is expressed as follows:

$$\begin{aligned} W_{\text{eff}}(\zeta) = 2a\Bigg[W\Bigg(& \mathrm{e}^{\left(a^2/W_1^2\right)\left[1+2\cos^2\zeta\right]} \\ & \times \frac{4a^2}{W_1 W_2}\mathrm{e}^{\left(a^2/W_2^2\right)\left[1+2\sin^2\zeta\right]}\Bigg)\Bigg]^{-\frac{1}{2}}, \end{aligned} \tag{B2}$$

where $W(\cdot)$ denotes the Lambert W function.[53]

The $R(x)$ denotes the scale function and the expression of the formula is shown below:

$$R(x) = \left[\ln\left(2\frac{1 - \exp\left(-a^2x^2/2\right)}{1 - \exp\left(-a^2x^2\right) I_0\left(a^2x^2\right)}\right)\right]. \tag{B3}$$

The $Q(x)$ denotes the shape function and the expression of the formula is shown below:

$$\begin{aligned} Q(x) = {} & 2a^2x^2\frac{\exp(-a^2x^2) I_1\left(a^2x^2\right)}{1 - \exp(-a^2x^2) I_0\left(a^2x^2\right)} \\ & \times \left[\ln\left(2\frac{1 - \exp\left(-a^2x^2/2\right)}{1 - \exp\left(-a^2x^2\right) I_0\left(a^2x^2\right)}\right)\right]^{-1}. \end{aligned} \tag{B4}$$

Acknowledgments

This work was supported by the Key Program of the National Natural Science Foundation of China (Grant No. 61531003), the National Natural Science Foundation of China (Grant No. 62001041), China Postdoctoral Science Foundation (Grant No. 2020TQ0016), and the Fund of State Key Laboratory of Information Photonics and Optical Communications.

References

[1] Gisin N, Ribordy G, Tittel W and Zbinden H 2014 *Rev. Mod. Phys.* **74** 145
[2] Scarani V, Bechmann-Pasquinucci H, Cerf N J, Dušek M, Lütkenhaus N and Peev M 2009 *Rev. Mod. Phys.* **81** 1301
[3] Xu F H, Ma X F, Zhang Q, Lo H K and Pan J W 2020 *Rev. Mod. Phys.* **92** 025002
[4] Pirandola S, Andersen U L, Banchi L, Berta M, Bunandar D, Colbeck R, Englund D, Gehring T, Lupo C, Ottaviani C, Pereira J L, Razavi M, Shaari J S, Tomamichel M, Usenko V C, Vallone G, Villoresi P and Wallden P 2020 *Adv. Opt. Photon.* **12** 1012
[5] Li Y M, Wang X Y, Bai Z L, Liu W Y, Yang S S and Peng K C 2017 *Chin. Phys. B* **26** 40303
[6] Zhu J, He G Q and Zeng G H 2007 *Chin. Phys. B* **16** 1364
[7] Shi J J, Li B P and Huang D 2020 *Chin. Phys. B* **29** 040301
[8] Grosshans F and Grangier P 2002 *Phys. Rev. Lett.* **88** 057902
[9] Weedbrook C, Lance A M, Bowen W P, Symul T, Ralph T C and Lam P K 2004 *Phys. Rev. Lett.* **93** 170504
[10] Qi B, Zhu W, Qian L and Lo H K 2010 *New J. Phys.* **12** 103042
[11] Jouguet P, Kunz-Jacques S, Leverrier A, Grangier P and Diamanti E 2013 *Nat. Photon.* **7** 378
[12] Pirandola S, Ottaviani C, Spedalieri G, Weedbrook C, Braunstein S L, Lloyd S, Gehring T, Jacobsen C S and Andersen U L 2015 *Nat. Photon.* **9** 397
[13] Weedbrook C, Ottaviani C and Pirandola S 2014 *Phys. Rev. A* **89** 012309
[14] Soh D B S, Brif C, Coles P J, Lütkenhaus N, Camacho R M, Urayama J and Sarovar M 2015 *Phys. Rev. X* **5** 041010
[15] Qi B, Lougovski P, Pooser R, Grice W and Bobrek M 2015 *Phys. Rev. X* **5** 041009
[16] Rupesh K, Hao Q and Romain Alléaume 2015 *New J. Phys.* **17** 043027
[17] Zhang Y C, Li Z Y, Chen Z Y *at al.* 2019 *Quantum Sci. Technol.* **4** 035006
[18] Zhang Y C, Chen Z Y, Pirandola S, Wang X Y, Zhou C, Chu B J, Zhao Y J, Xu B J, Yu S and Guo H 2020 *Phys. Rev. Lett.* **125** 010502
[19] Arnold T, Tyrnita M, Keith D and Ronald M 2010 *Proceedings of SPIE 7815, Quantum Communications and Quantum Imaging VIII*, August 30, 2010, San Diego, California, United States, p. 179
[20] Fedrizzi A, Ursin R, Herbst T, Nespoli M, Prevedel R, Scheidl T, Tiefenbacher F, Jennewein T and Zeilinger A 2009 *Nat. Phys.* **5** 389
[21] Buttler W T, Hughes R J, Kwiat P G, Lamoreaux S K, Luther G G, Morgan G L, Nordholt J E, Peterson C G and Simmons C M 1998 *Proceedings of SPIE 3385, Photonic Quantum Computing II*, July 6, 1998, Orlando, FL, United States, p. 14
[22] Liao S K, Yong H L, Liu C, *at al.* 2017 *Nat. Photon.* **11** 509
[23] Lorenz S, Rigas J, Heid M, Andersen U L, Lütkenhaus N and Leuchs G 2006 *Phys. Rev. A* **74** 042326
[24] Heim B, Elser D, Bartley T, Sabuncu M, Wittmann C, Sych D, Marquardt C and Leuchs G 2010 *Appl. Phys. B* **98** 635
[25] Heim B, Peuntinger C, Killoran N, Khan I, Wittmann C, Marquardt C and Leuchs G 2014 *New J. Phys.* **11** 113018
[26] Lorenz S, Korolkova N and Leuchs G 2004 *Appl. Phys. B* **79** 273
[27] Elser D, Bartley T, Heim B, Wittmann C, Sych D and Leuchs G 2009 *New J. Phys.* **11** 045014
[28] Peuntinger C, Heim B, Müller C R, Gabriel C, Marquardt C and Leuchs G 2014 *Phys. Rev. Lett.* **113** 060502
[29] Shen S Y, Dai M W, Zheng X T, Sun Q Y, Guo G C and Han Z F 2019 *Phys. Rev. A* **100** 012325
[30] Barbosa G A, Corndorf E, Kumar P and Yuen H P 2002 *Proceedings of SPIE 4821, Free-Space Laser Communication and Laser Imaging II*, December, 9, 2002, Seattle, WA, United States, p. 409
[31] Wang L, Zhao S M, Gong L Y and Cheng W W 2015 *Chin. Phys. B* **24** 120307
[32] Ricklin J C, Hammel S M, Eaton F D and Lachinova S L 2006 *J. Opt. Fiber Commun. Rep.* **3** 111
[33] Majumdar A K and Ricklin J C 2005 *Proceedings of SPIE 5892, Free-Space Laser Communications V*, September 12, 2005, San Diego, California, United States, p. 149
[34] Vidiella-Barranco A and Borelli L F M 2006 *Int. J. Mod. Phys. B* **20** 1287
[35] Bowen W P, Treps N, Schnabel R, Ralph T C and Lam P K 2003 *J. Opt. B-Quantum S. O.* **5** S467
[36] Schaefer B, Collett E, Smyth R, Barrett D and Fraher B 2007 *Am. J. Phys.* **75** 163
[37] Shen S Y, Zheng X T, Guo G C and Han Z F 2020 *Opt. Lett.* **45** 2592
[38] Gu W Y, Zhao S H, Dong C, Zhu Z D and Qu Y Y 2019 *Acta Phys. Sin.* **68** 090302 (in Chinese)
[39] Zhang S J, Ma H X, Wang X, Zhou C, Bao W S and Zhang H L 2019 *Chin. Phys. B* **28** 80304
[40] Zhang S J, Xiao C, Zhou C, Wang X, Yao J S, Zhang H L and Bao W S 2020 *Chin. Phys. B* **29** 20301
[41] Xie C L, Guo Y, Wang Y J, Huang D and Zhang L 2018 *Chin. Phys. Lett.* **35** 090302
[42] Zhang X G and Zheng Y 2008 *Chin. Phys. B* **17** 2509
[43] Wang S Y, Huang P, Wang T and Zeng G H 2018 *New J. Phys.* **20** 083037
[44] Vasylyev D, Semenov A A and Vogel W 2016 *Phys. Rev. Lett.* **117** 090501
[45] Ghoname S, Fayed H A, El A, Ahmed A and Aly M H 2014 *Iran. J. Sci. Technol. Trans. Electr. Eng.* **44** 119
[46] Vasylyev D, Semenov A A, Vogel W and Günthner K and Thurn A, Bayraktar Ö and Marquardt C 2017 *Phys. Rev. A* **96** 043856
[47] Ali M 2015 *IOSR J. Appl. Phys.* **7** 16
[48] Esmail M A, Fathallah H and Alouini M S 2016 *Proceedings of IEEE International Conference on Communications Workshops*, May 23–27, 2016, Kuala Lumpur, Malaysia, p. 151
[49] Korolkova N, Leuchs G, Loudon R, Ralph T C and Silberhorn C 2002 *Phys. Rev. A* **65** 052306
[50] Heid M and Lütkenhaus N 2006 *Phys. Rev. A* **73** 052316
[51] Kim I I, Mcarthur B and Korevaar E J *Proceedings of SPIE 4214, Optical Wireless Communications III*, February 6, 2001, Boston, MA, United States, p. 26
[52] Padhy J B, Satarupa A and Patnaik B 2020 *The Effect of Atmosphere on FSO Communication at Two Optical Windows Under Weather Condition of Bhubaneswar City* (Singapore: Springer) p. 417
[53] Corless R M, Gonnet G H, Hare D E, Jeffrey D J and Knuth D E 1996 *Adv. Comput. Math.* **5** 329